Rev.Adv.Mater.Sci. 9 (2005) 109-129

FABRICATION OF METAL NANOPARTICLES IN SAPPHIRE BY LOW-ENERGY ION IMPLANTATION

A.L. Stepanov[1] and I.B. Khaibullin[2]

[1]Institute of Physics and Erwin Schrödinger Institute for Nanoscale Research, Karl-Franzens-University Graz, A-8010 Graz, Austria
[2]Kazan Physical-Technical Institute, Russian Academy of Sciences, Sibirsky Trakt 10/7, 420029 Kazan, Russian Federation

Received: March 17, 2005

Abstract. The present review concentrates on the fabrication of metal nanoparticles in sapphire matrix by ion implantation and their modification by laser annealing. This approach is promising for the development of optical composite materials in the optoelectronics production technology. Composite layers were fabricated in sapphire by implantation of 40-keV Cu^+ ions at a dose of $1.0 \cdot 10^{17}$ ion/cm^2 and an ion beam current density varying from 2.5 to 10 μA/cm^2. The composites were examined by different methods: Rutherford backscattering (RBS), atomic force microscopy (AFM) and optical spectroscopy. It is shown that ion implantation is suited for creation of copper nanoparticles in the near-surface sapphire layer. However, the nanoparticle size distribution in this layer is nonuniform. An interaction of high power excimer laser pulsed with fabricated composite layer aimed to modify the sizes and the size distribution of copper particles. It is found that the laser annealing diminishes nanoparticles in the sapphire. Experimental data on laser modification may be explained by photofragmentation and/or melting of the nanoparticles in the sapphire matrix.

1. INTRODUCTION

Composite materials, such as dielectrics with embedded metal nanoparticles (MNPs), are promising optoelectronic materials. An example of their application in optoelectronics is a prototype of integrated electronic circuit - chip that combines metallic wires as conductors of electric signals with fibers as guides of optical signals. In practice, light guides are frequently made of synthetic sapphire (Al_2O_3) or silicon oxide, which are deposited on or buried in semiconductor substrates (Fig. 1). In this case, electrooptic emitters and that accomplish electric-to-optic signal conversion are fabricated inside the dielectric layer. This light signal from a microlaser is focused in a light guide and then transmitted through the optoelectronic chip to a high-speed photodetector, which converts the photon flux to the flux of electrons. It is expected that light guides used instead of metallic conductors will improve the data rate by at least two orders of magnitude. Moreover, there is good reason to believe that optical guide elements will reduce the energy consumption and heat dissipation, since metallic or semiconductor components of the circuits may be replaced by dielectric ones in this case. Prototype optoelectronic chips currently available are capable of handling data streams with a rate of 1 Gbit/s, with improvement until 5 Gbit/s in future.

Key elements of dielectric waveguides used for light propagation are nonlinear optical switches, which must provide conversion of laser signal for pulse duration as short as pico- or even femtoseconds. The nonlinear optical properties of MNP-containing dielectrics stem from the dependence of their refractive index on incident light intensity [1,2]. This effect is associated with MNPs, which exhibit an enhancement of local electromagnetic field in a composite and, as consequence, a high value of the third order nonlinear susceptibility when exposed to ultrashort laser pulses. Therefore, such MNP-containing dielectric materials may be used to advan-

Corresponding author: A.L. Stepanov, e-mail: andrey.stepanov@uni-graz.at ; anstep@kfti.knc.ru

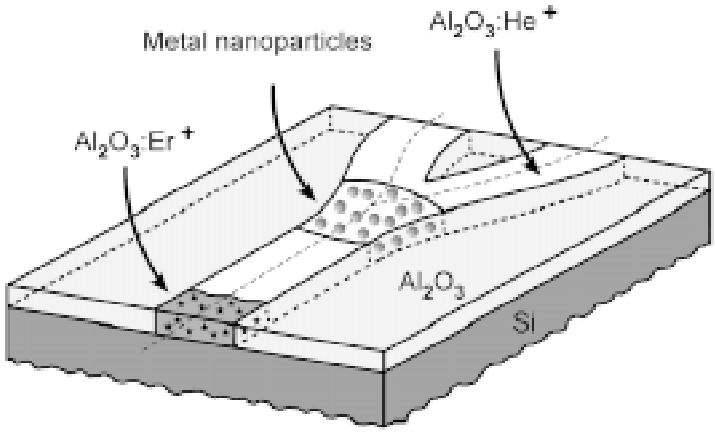

Fig. 1. A prototype of optoelectronic chip with sapphire waveguide on silicon substrate. Ion implantation can be applied to form selective area doped by rear metal ions (illustrated by stars) to work as micro laser and to saturate waveguide, created by He-ion irradiation with metal nanoparticles to form an optical switcher.

tage in integrated optoelectronic devices, for example, as shown in Fig. 1.

It is well known [1] that a local field enhancement in MNPs stimulates a strong linear optical absorption called as surface plasmon resonance (SPR). The electron transitions responsible for plasmon absorption in MNPs cause also a generation of an optical nonlinearity of a composite in the same spectral range. As a result, the manifestation of nonlinear optical properties is most efficient for wavelengths near the position of a SPR maximum. In practice, to reach the strong linear absorption of a composite in the SPR spectral region, attempts are made to increase the concentration (filling factor) of MNPs. Systems with a higher filling factor offer a higher nonlinear susceptibility, when all other parameters of composites being the same [1].

There is variety of ways to synthesis MNPs in dielectrics, such as magnetron sputtering, the convective method, ion exchange, sol–gel deposition, *etc*. One of the most promising enhanced fabrication methods is ion implantation (II) [3,4] because it by ion implantation allows reaching a high metal filling factor in an irradiated matrix beyond the equilibrium limit of metal solubility and provides controllable synthesis of MNPs at various depths under the substrate surface. Nearly any metal–dielectric composition may be produced using II. This method allows the strict control of the doping ion beam position on the sample surface with implant dose as, for example, in the case of ion-beam lithography.

Today, II is widely used in industrial semiconductor chip fabrication. Therefore, the combination of MNP-containing dielectrics with semiconductor substrates by same technological approach as II could be reached quite effective. Moreover, II can be applied for different steps in optoelectronic material fabrication such as creation of optical waveguides by implantation with rear gas ions (H^+,He^+, *etc.*) [3], a designing of electric-to-optic signal convectors and microlaser by irradiation of dialectics waveguides with rear metal ions (Er^+, Eu^+, *etc.*) [3,5] and a synthesis of metal nanoparticles as discussing in this article (Fig. 1).

The history of MNP synthesis in dielectrics by II dates back to 1973, when a team of researchers J. Davenas *et al.* at the Lyons University (France) pioneered this method to create particles of various metals (silver, sodium, calcium, *etc.*) in LiF and MgO ionic crystals [6,7]. Later, in II practice MNPs were successfully fabricated in various materials, such as polymers, glass, artificial crystals, and minerals. In this work, the ion synthesis of MNPs in synthetic sapphire (Al_2O_3) is considered, since this substrate as a dielectric matrix containing MNPs has been studied to a much smaller degree than standard optical waveguide materials, e.g., silicon dioxide.

As follows from the currently available publications concerning ion synthesis of MNPs in Al_2O_3 [8–59] (see table referenced until 2005 year), this matrix as a basis for a composite was of interest for a long time since a work on Fe^+-ion implantation in 1987 from C.J. McHargue *et al.* [8] and M. Ohkubo *et al.* [13]. The table lists the types of MNPs and conditions of their synthesis directly by II or by II combined with heat treatments. As seen in a dia-

Table. Types of metal nanoparticles and conditions for their synthesis in Al_2O_3 by ion implantation combined with post-implantation heat treatments. (Abbreviations – TEM, transmission electron microscopy; XPS, X-ray photoelectron spectroscopy; CEMS, conversion electron Mossbauer spectroscopy; XRD, X-ray diffraction; VSM, vibrating sample magnetometry; RM, resistive measurements; GIXRD, glancing incidence X-ray diffraction; SQUID, superconducting quantum-interference-device, magnetometer; OS, optical spectroscopy; AFM, atomic-force microscopy; MR, magnetoresistance measurements; and LFRS, low frequency Raman scattering; $\chi^{(3)}$ DFWM, measurements of the third-order nonlinear optical susceptibility by a degenerate four-wave mixing. The ions are listed in the order they follow in the Periodic Table of elements).

Metal of particles	Matrix type	Ion beam energy, keV	Ion dose ion/cm^2	Ion curent density, μA/см^2	Matrix temeperature, °C	Post-implantation heat treatment	Methods of particle indefication	Authors
α-Fe	α-Al_2O_3 [0001]	100 160	$4.0\cdot10^{16}$ $7.0\cdot10^{16}$ $2.0\cdot10^{17}$		-200 25		TEM, X-ray, CEMS	McHargue *et al.* 1987 [8] 1990 [9] 1991 [10] 1996 [11] 1998 [12]
α-Fe	α-Al_2O_3 [0001]	400	$1.0\cdot10^{17}$		240	Annealing in vacuum at 700-1200 °C for 1 h.	TEM, XRD VSM	Ohkubo *et al.* 1987 [13] 1989 [14]
α-Fe	α-Al_2O_3 [0001]	160	$4.0\cdot10^{16}$		45	Annealing in Ar-4% H_2 at 1500 °C for 1 h.		Farlow *et al.* 1990 [15]
α-Fe	α-Al_2O_3 polysrict.	110	$1.0\cdot10^{17}$	10	25		TEM	Donnet *et al.* 1991 [16]
α-Fe	α-Al_2O_3 [0001]	160	$1.0\cdot10^{17}$	2	25			Sklad *et al.* 1992 [17]
Fe	α-Al_2O_3 polycrist.	60	$(0.2–1.2)\cdot10^{17}$	2				Jang *et al.* 1997 [18]
Fe	Al_2O_3 [0001]	85	$4.0\cdot10^{16}$ $7.0\cdot10^{16}$ $1.0\cdot10^{17}$	10-15	25		RM	Kobayashi et al 1998 [19]
Fe	Al_2O_3	380	$1.0\cdot10^{17}$ $4.0\cdot10^{17}$ $1.0\cdot10^{18}$	2			RM	Kobayashi, Terai 1998 [20]

α-Fe	α-Al_2O_3	100	$(1.0\text{-}2.0)\cdot10^{17}$	2-3	25		CEMS	Sakamoto *et al.*1999 [21] Hayashi *et al.* 2002 [22] Wakabayashi *et al.* 2002 [23]
Fe	α-Al_2O_3 [0001] [1120]	160	$1.0\cdot10^{17}$ $4.0\cdot10^{17}$		25		TEM, GIXRD, VSM	Alves *et al.* 2002 [24]
Fe	α-Al_2O_3	160	$1.0\cdot10^{17}$ $4.0\cdot10^{17}$					Monteiro *et al.* 2002 [25]
Fe	Al_2O_3	350	$1.0\cdot10^{17}$		-200 25	Annealing in Ar-4% H_2 at 1100 °C for 2 h.	X-ray TEM, SQUID	White *et al.* 2003 [26]
α-Fe	α-Al_2O_3 [0001]	150	$1.0\cdot10^{17}$		25		TEM, CEMS	McHargue *et al.*2004 [27]
α-Fe	α-Al_2O_3 [0001]	150	$1.0\cdot10^{17}$		25 1000	Annealing in Ar-4% H_2 at 1100 °C for 1 h.	TEM, CEMS	McHargue *et al.*2004 [27]
Co	α-Al_2O_3	20	$(0.5\text{-}5.0)\cdot10^{17}$		25			Saito *et al.* 1991 [28]
Co	α-Al_2O_3 <0001> <0221> <1120>	150	$5.0\cdot10^{17}$		25		SQUID, OS	Marques *et al.* 2001 [29] 2002 [30]
Co	Al_2O_3	140	$8.0\cdot10^{16}$		25 -100	Annealing in Ar-4% H_2 at 1100 °C for 2 h	TEM, X-Ray, SQUID	Meldrum *et al.* 2003 [31]
Ni	α-Al_2O_3 [0001]	160	$4.0\cdot10^{16}$		45	Annealing in Ar-4% H_2 at 1500 °C for 1 h.		Farlow *et al.*1990 [15]
Ni	Al_2O_3 [1120]	3000	$1.6\cdot10^{18}$	1	20-250		MR	Kobayashi et al.1996 [32]
Ni	α-Al_2O_3	64	$1.0\cdot10^{17}$	0.5			TEM, X-ray	Xiang *et al.*2004 [33] 2004 [34]
Cu	α-Al_2O_3 polysrict.	110	$1.0\cdot10^{17}$	10	25		TEM	Donnet *et al.*1991 [16]
Cu	Al_2O_3	160	$(0.2\text{-}.0)\cdot10^{17}$	< 2		Annealing in air at 673 °C for 1 h		Ila *et al.* 1998 [35]

Cu	Al_2O_3	2100	$1.0 \cdot 10^{17}$		-170	Annealing in vacuum at 770-1270K for 1 h		Ikeyama *et al.* 2001 [36] 2002 [37]
Cu	Al_2O_3	40	$1.0 \cdot 10^{17}$	2.5-10	25		OS, AFM	Stepanov *et. al* 2001 [38] Stepanov 2002 [39] Stepanov *et. al* 2002 [40] Stepanov, Popok 2003 [31] Stepanov 2004 [42]
Zr	α-Al_2O_3 polycryst.	110	$1.0 \cdot 10^{17}$	10	25		TEM, X-ray	Donnet *et al.*1991 [16]
Pd	α-Al_2O_3 polycryst.	2	$(1.0\text{-}5.0) \cdot 10^{16}$	0.5	1.0		XPS	Battaglin *et al.*1999 [43]
Ag	Al_2O_3	50	$(0.4\text{-}1.9) \cdot 10^{17}$	1-5	25 -200		OS	Rahmani *et al.* 1988 [44] Rahmani, Townsend 1989 [45]
Ag	Al_2O_3 [0001]	1800	$1.2 \cdot 10^{17}$		-200	Annealing in air at 1100° C for 2 h	TEM, OS, $\chi^{(3)}$ DFWM	White *et al.* 1992 [46] 1993 [47]
Ag	Al_2O_3	1500	$(0.2\text{-}2.0) \cdot 10^{17}$	< 2		Annealing in air at 773° C for 1 h.		Ila *et al.* 1998 [35]
Ag	Al_2O_3	25-30	$(0.2\text{–}2.0) \cdot 10^{17}$	0.6-6.2	25			Steiner *et al.* 1998 [48]
Sn	Al_2O_3	160	$(0.2\text{-}2.0) \cdot 10^{17}$	< 2		Annealing in air at 773 °C for 1 h.		Ila *et al.* 1998 [35]
Pt	Al_2O_3 [0001]	160	$5.0 \cdot 10^{16}$	0.4	25			Alves *et al.* 1999 [49]
Pt	Al_2O_3	910	$8.2 \cdot 10^{16}$		200	Annealing in Ar-4% H_2 at 1100 °C for 2 h.	X-ray TEM, SQUID	White *et al.* 2003 [26]
Au	Al_2O_3 [0001]	400	$6.8 \cdot 10^{16}$		1200		TEM	Ohkubo, Suzuki. 1988 [50]
Au	Al_2O_3 [0001]	2750 3000	$(1.0\text{-}1.2) \cdot 10^{17}$		-200	Annealing in Ar-4% H_2 at 900-1100 °C for 1-20 h	TEM, OS, $\chi^{(3)}$ DFWM	White *et al.* 1992 [45] 1993 [46]

Au	Al_2O_3 [0001]	2750	$2.2 \cdot 10^{16}$			Annealing in Ar+4%H_2 at 1100 °C 1 h.		Henderson *et al.* 1995 [51]
Au	Al_2O_3	2000	$(0.2\text{-}2.0) \cdot 10^{17}$	< 2		Annealing in air at 973-1323 °C for 1 h.		Ila *et al.* 1998 [36]
Au	Al_2O_3	160	$1.0 \cdot 10^{17}$				OS	Marques *et al.* 2004 [52]
Au	c-Al_2O_3	1800	$(0.1–1.0) \cdot 10^{18}$	1.2		Annealing at 1000 °C and 1200°C for 1 h	OS, LFRS	Dhara et al. 2004 [53]
Eu	Al_2O_3	400	$1.0 \cdot 10^{16}$	8 16	34	Annealing in air at 1200 °C for 1 h		Can *et al*. 1994 [54] 1995 [55]
FeCo	α-Al_2O_3	100	$(1.0\text{-}2.0) \cdot 10^{17}$	2-3	25		CEMS VSM, MR	Sakamoto *et al.* 1999 [21] Hayashi *et al.* 2002 [22] 2003 [56]
FePt	α-Al_2O_3	Fe-350 Pt-910	Fe-$1.0 \cdot 10^{17}$ Pt-$(0.5\text{-}1.1) \cdot 10^{17}$		Fe– 200-550 Pt-200,500	Annealing in Ar+4% H_2 at 1100 °C for 2 h	SQUID, TEM, X-ray	Vallet *et al.* 2002 [57] White *et al.* 2002 [58] 2003 [26]
CoPt	α-Al_2O_3	Co-325 P-910	$(0.5\text{-}1.0) \cdot 10^{17}$		200, 500	Annealing in Ar+4% H_2 at 1100 °C for 2 h	SQUID, TEM, X-ray	Withrow *et al*. 2003 [59]

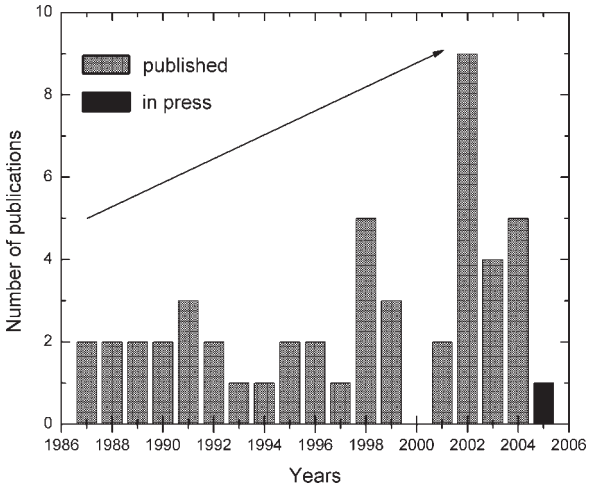

Fig. 2. Attendance of papers in the literature on synthesis of metal nanoparticles in sapphire matrix by ion implantation until 2005 year.

gram (Fig. 2), a number of publications on MNPs fabrication in Al_2O_3 by II continuously increases during last years. This fact clearly demonstrates a wide interest in the study of this topic; various scientific groups are working now in this field and Kazan Physical-Technical Institute of the Russian Academy of Sciences, Instituto Tecnologe Nuclear (Portugal), University of Tennessee-Knoxville and Oak Ridge National laboratory (USA), Musashi Institute of Technology (Japan), Goteborg University and Chalmers University of Technology (Sweden) should be mentioned as the active participants of these investigations.

As seen in the Table, while MNP synthesis in Al_2O_3 has been extensively explored, there are only few studies [26,35,36,44-53] devoted to the formation of noble metal particles, which are the most effective in terms of nonlinear optical properties. For nonlinear optics, copper, which is close to noble metals accord to the high concentration of the conductive electrons, is the most preferable material [1,2]. However, as follows from the Table, ion synthesis of copper nanoparticles in Al_2O_3 without using auxiliary post-implantation heat treatments has not been implemented for long time. The feasibility of creating composites by low energy implantation (<100 keV) of copper ions into a single-crystal sapphire substrate was recently demonstrated by A. Stepanov *et al.* in 2001 [38-42]. It should be noted that the early attempts to create composites by irradiation of Al_2O_3 with high accelerated (~ 130 keV–2.4 MeV) copper ions [60-64] failed (copper particles did not form); therefore, those works are omitted from the table. Subsequent heat treatment of the substrates irradiated by high energy ions in those works causes, along with the formation of copper nanoparticles, the growth of copper oxide particles and $CuAl_2O_4$ spinel phase [36,37]. Of special interest is the research [16], where copper nanoparticles were synthesized in polycrystalline Al_2O_3 by moderate low energy (110 keV) implantation. However, the polycrystalline state of sapphire is strongly different from the single-crystalline one: an elevated density of structure defects, specifically, grain (domain) boundaries, in the former changes radically the synthesis conditions of MNPs. Therefore, though mentioned in the table, work [16] is beyond the scope of this review.

Thus, present review covers publications devoted to ion synthesis of copper nanoparticles of a desired size in a sapphire substrate. Since the linear and nonlinear optical properties of MNPs are directly related to their sizes [65], one may control the optical performance of a composite as a whole by controllably varying the MNP size and MNP size distribution. One way of changing the particle size distribution while keeping a high value of the filling factor in substrate is to anneal the composite by high power excimer laser pulses [66–73]. Emphasis in this work will be on modification of MNPs in Al_2O_3 synthesized by II during exposing the composite by laser radiation.

2. EXPERIMENTAL PROCEDURE

Thin wafers of synthetic polycrystalline sapphire, which offers a high optical transparency in the spectral range 200–1000 nm, were used as substrates. The plane exposed to radiation was (1012). Wafers were implanted with 40 keV Cu^+ ions at a dose of $1 \cdot 10^{17}$ ion/cm^2 and an ion beam current density varying from 2.5 to 12.5 mA/cm^2. Experiments were carried out with an ILU-3 implanter under a controlled vacuum of 10^{-5} Torr (Fig. 3). Prior to implantation, the substrate was kept at room temperature; in the course of implantation, it was continuously cooled by running water.

The implanted samples were analyzed by Energy-Dispersive X-Ray (EDX) spectroscopy at the accelerating voltage of 20 keV by a scanning electron microscope (REMMA-202M) and by Rutherford backscattering (RBS) using a beam the of $^4He^+$ ions with energy of 2 MeV by a van de Graaf accelerator. Energy spectra from a collimated solid-state detector (laboratory scattering angles of 120° and 170°) were evaluated to yield profiles of absolute concentration versus depth in the sample using the Data

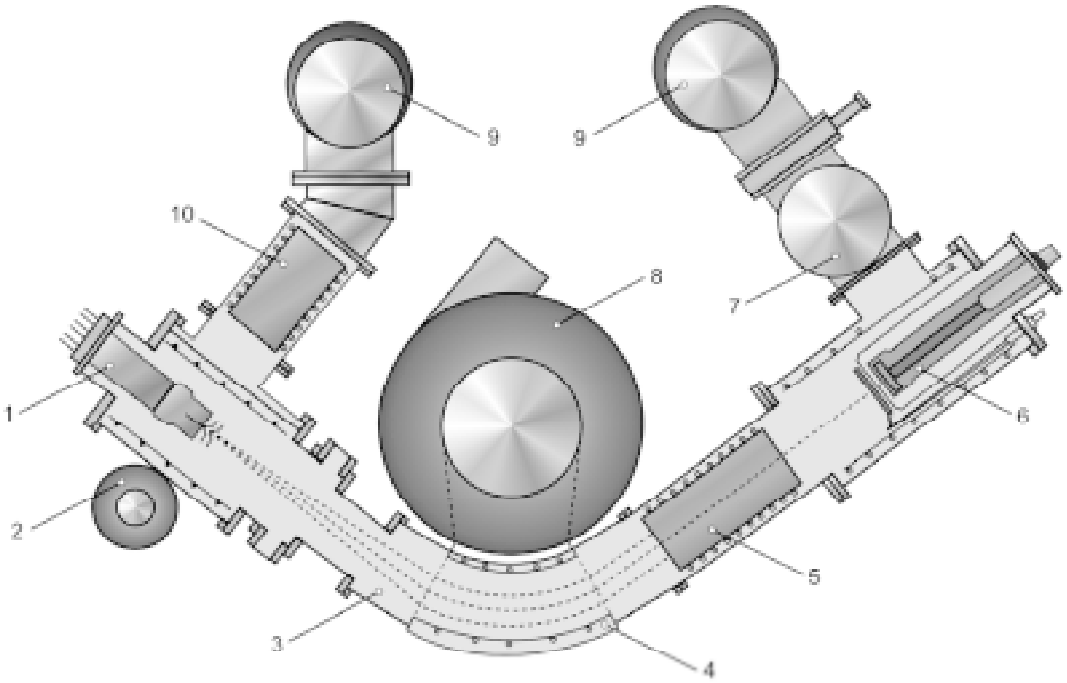

Fig. 3. Overview of the ion implanter ILU-3: (1) ion source; (2) electromagnet of the ion source; (3) vacuum chamber; (4) water cooling system; (5) nitrogen cooled trap; (6) ion receiver and target holder; (7) forevacuum pump; (8) electromagnet of the sector ion analyzer; (9) diffusion pumps; (10) water cooled trap.

Furnace computer program [74]. Optical reflection spectra were recorded with a Monolight one-beam fiber-optic device in the range 380–800 nm at normal incidence of the radiation on the sample. The optical transmission in the range 200–1000 nm was measured with a Perkin Elmer Lambda 19 double-beam spectrophotometer.

Pulsed laser annealing of the implanted Al_2O_3 substrate was done by a KrF excimer laser (ALTEX 210) at a wavelength of 248 nm and pulse duration of 25 ns. Ten pulses of equal energy density (0.3 J/cm^2) were accumulated in the same area of the sample at a repetition rate of 1 Hz. Pulse-to-pulse energy variation was typically within ±2%. The energy density was controlled with a laser power meter DGX FL150A-EX-RP. To improve the laser radiation uniformity, the light beam, before normal incidence on the sample surface, was passed through a circular diaphragm of diameter 2 mm. The laser annealing was carried out in ambient atmosphere at room temperature. Since the irradiation area was quite small (the light beam was limited by the diaphragm), annealed samples were analyzed by means of optical reflection spectroscopy.

Topographic profiling of the as-implanted and laser annealed surface was performed with an atomic force microscope (AFM) Solver-P4, working in tapping mode. Vertical displacement of the sensitive cantilever in the microscope was registered by deflection of the lower power laser beam reflected from the probe tip. The samples were clamped on a tube piezoscanner providing as canning area of 3.7×3.7 μm^2 and they were measured in an air environment. The constant force-operating mode was employed and a conventional feedback loop circuit was used to maintain the constant force at less than 100 nN.

3. ION SYNTHESIS OF METAL NANOPARTICLES IN DIELECTRIC MATRIX BY LOW ENERGY ION IMPLANTATION

Ion implantation is an effective technological tool for introducing single impurities into the surface layer of the substrate to a depth of several micrometers [3]. The degree of surface modification of the materials depends on their individual chemical and structural properties, as well as on variations of II parameters, such as the type and energy of an implant, current density in ion beam, substrate temperature, *etc*. A critical implantation parameter is ion dose F_0, which determines the implant amount. Depending on the modification of a dielectric target by irradiation, II can be conventionally divided into low-dose and high-dose processes (Fig. 4).

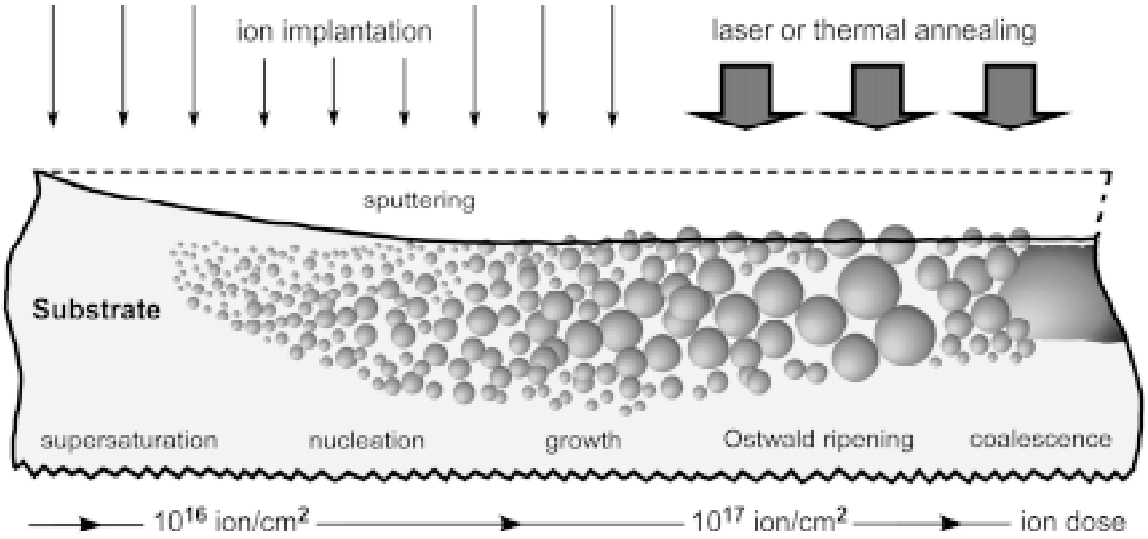

Fig. 4. Basic physical processes (from left to right) involved in the formation of nanoparticle from an implant vs. the ion dose with regard to surface sputtering under irradiation.

In the case of low-dose II ($\sim F_0 \leq 5.0 \cdot 10^{14}$ ion/cm^2), the ions implanted, after stopping and thermalization, are dispersed throughout the volume of the dielectrics and are well separated from each other. The energy of the implant is transferred to the matrix via electron shell excitation (ionization) and nuclear collisions. This causes radiation-induced defects, which, in turn, may reversibly or irreversibly modify the material structure [3]. Various types of crystal structure damage have been observed in practice [3]: extended and point defects, amorphization and local crystallization, precipitation of a new phase made up of host atoms or implanted ions, *etc*. In addition, II may be accompanied by the effective sputtering of the surface of the dielectric target, as observed for example in the case of Cr^+ and Ti^+ implantation into Al_2O_3 by photon tunnel microscopy (Fig. 5) [75], or Cu^+ implantation into the $MgAl_2O_3$ spinel matrix and SiO_2 glass [76]. Sometimes, sputtering competes with swelling, as

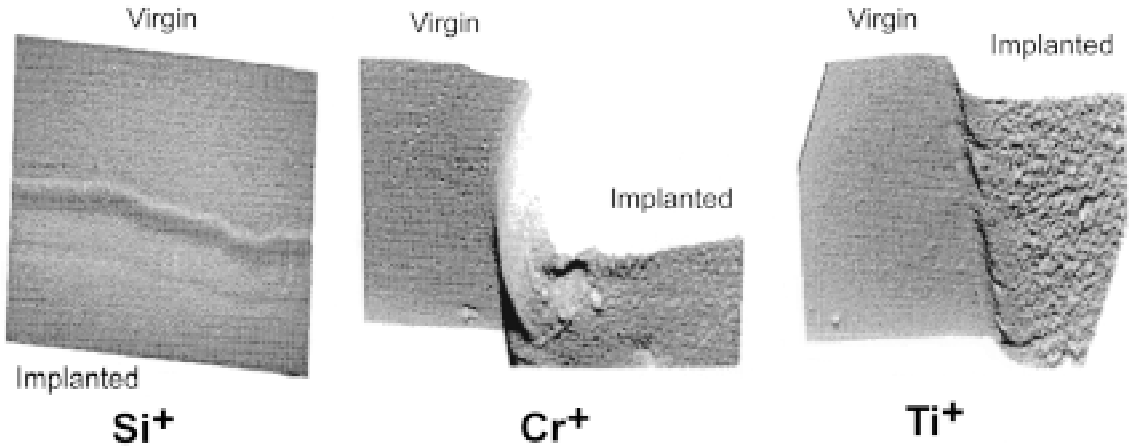

Fig. 5. Three-dimensional photon tunnel microscope image of sapphire implanted with $3.0 \cdot 10^{17}$ ions/cm^2 at 160 KeV, at edge of mask showing sputtered region. Fragment of image is taken with contrast correction from [75].

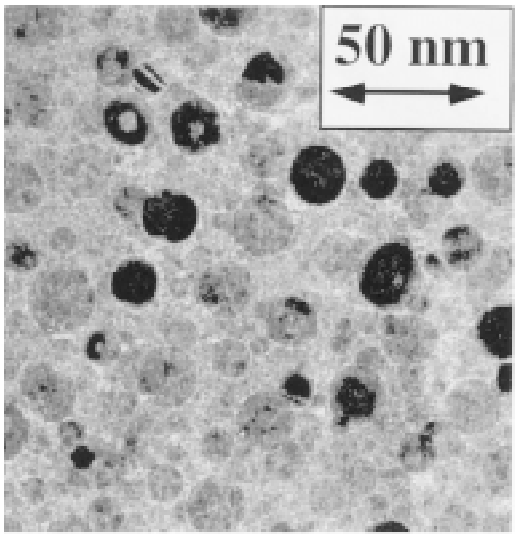

Fig. 6. Micrograph of metal nanoparticles produced by 160-keV Cu^+ implantation into SiO_2 at a dose of $6.0 \cdot 10^{16}$ ion/cm^2; fragment of picture from [79].

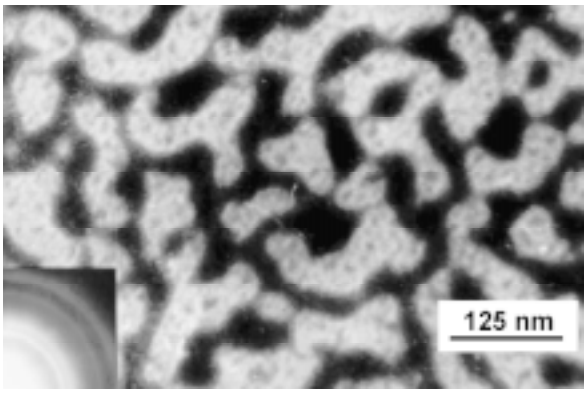

Fig. 7. Micrograph of cobalt labyrinth structures produced by Co^+ implantation into epoxy resins at a dose of $2.5 \cdot 10^{17}$ ion/cm^2 [83].

in the case of spinel and glasses exposed to extremely high current beams of metal ions [76], in the case of inert gas ions embedded in polymers [77] or some semiconductors irradiated by various ions with high doses [78].

The range of high-dose implantation may be divided into two characteristic dose (irradiation time) sub-ranges (Fig. 4). In the range $10^{15} \le \sim F_0 \le 10^{17}$ ion/cm^2, the implant concentration exceeds the solubility limit of metal atoms in dielectrics (in particular, in sapphire) and the system relaxes by nucleation and growth of MNPs, as illustrated in SiO_2 glass (Fig. 6) [79]. The boundary dose value depends on the type of the dielectric matrix and implant. For example, for 25-keV Ag^+-ion implantation into $LiNbO_3$, the boundary dose was found to be $F_0 \sim 5.0 \cdot 10^{15}$ ion/cm^2 [80], for 30-keV silver ions embedded in solid state epoxy resin, $F_0 \sim 10^{16}$ ion/cm^2 [81], but a formation of ultra-dispersed magnetic phase in polyimide was found to form under fluencies as high as $\sim 10^{17}$ ion/cm^2 at 40-keV iron ions irradiation [82]. The boundary dose (at which MNPs nucleate) for copper implantation into Al_2O_3 has not been reported in the literature yet.

The next subrange of high-dose implantation, $\sim F_0 \ge 10^{17}$ ion/cm^2, leads to the coalescence of already existing MNPs with the formation of either MNP aggregates or thin quasi-continuous films at the dielectric surface (Fig. 4). For instance, the irradiation of epoxy resin by 40-keV cobalt ions at higher-than threshold-nucleation doses favors the formation of thin labyrinth structures (Fig. 7) [83]. The MNP distribution established in the dielectrics after coalescence or Ostwald ripening may be dramatically disturbed by postimplantation thermal or laser annealing [3].

The works considered in this review were aimed at studying composites consisting of the sapphire matrix with isolated copper nanoparticles; i.e., the particles were synthesized by high-dose ($F_0 \sim 10^{17}$ ion/cm^2) II. For the case of Cu^+-ions implantation with a moderate low energy (40 keV), elastic ion energy losses causes oxygen and aluminum atom displacements from the crystallographic positions in the matrix and chemical bond breaking. It is known that implantation of various metal ions into the crystalline Al_2O_3 matrix leads to the amorphization of the ion-doped layer at relatively low doses (on the order of 10^{15} ion/cm^2) [3,84].

Accumulation of an implant in the irradiated matrix is a gradual long-term process during II. The implant distribution in the target is routinely described with the TRIM algorithm applied to the statistical Gaussian distribution, which has a symmetric statistical profile [85]. However, as was shown earlier [86–89], the TRIM algorithm works correctly in describing the metal atom distribution across the dielectric for low-energy (< 100 keV) II only if the ion dose is very low (<< 10^{15} ion/cm^2). This is because TRIM algorithm ignores the effect of dynamic surface sputtering (Figs. 2 and 4) and alterations of the ion range due to the variation of the target atomic composition of the substrate with the amount of the implant accumulated. Therefore, the dynamic computer code DYNA was suggested to be more appropriate for simulating the copper distribution in Al_2O_3 [87,88]. DYNA algorithm is based on binary collision approximations in intermixed surface layer

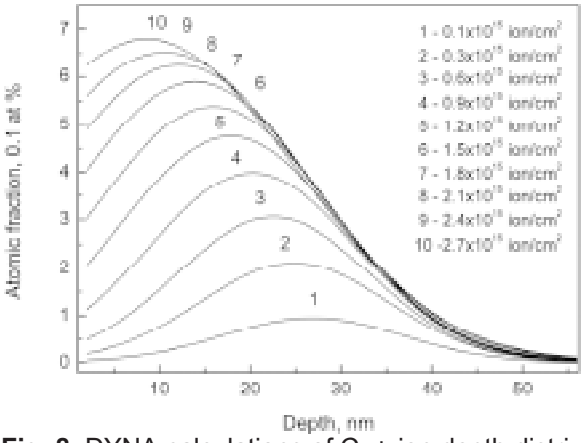

Fig. 8. DYNA calculations of Cu+-ion depth distribution for 40 keV implantation in Al_2O_3 with different doses.

between the implant and substrate atoms. Dynamic target sputtering and changes of the near-surface layer composition due to cascade atomic mixing in dependence on irradiation time are also considered.

Dynamic formation of a non-symmetrical depth distribution of implanted Cu^+ ions in Al_2O_3 according to DYNA calculations is presented in Fig. 8. It can be seen from this figure that the implant distribution varies with the implantation time, i.e., Fig. 8 visualizes the copper accumulation in substrate. At low doses ($F_0 \leq 0.1 \cdot 10^{15}$ ion/cm^2), the DYNA- and TRIM-based distributions are quite similar (curve 1). However, as the dose grows up to approximately $2.5 \cdot 10^{15}$ ion/cm^2, the Gaussian profile changes to an asymmetric curve and the implant concentration maximum shifts closer to the irradiated surface. From a dose of ~ $3.0 \cdot 10^{15}$ ion/cm^2, the copper profile in depth of the sapphire is stabilized, i.e., becomes dose-independent. This value manifests the upper bound for the domain of applicability of the DYNA algorithm. At higher doses, the implant concentration in the surface layer will exceed the limiting solubility of copper in sapphire [3] with regard to a low ion energy (40 keV), which DYNA cannot take into account.

4. FORMATION OF COPPER NANOPARTICLES IN SAPPHIRE BY HIGH-DOSE ION IMPLANTATION

In the case of implantation by Cu^+ ions at relatively low energy 40 keV, nuclear collisions prevail during interaction of accelerated ions with atoms of substrate, but along with this, target Al_2O_3 atoms also effectively lose electrons. As a result of interaction with these electrons, the Cu^+ ions deionize with the formation of neutral copper atoms Cu^0. They displace atoms in the sapphire matrix and break some of chemical bonds of substrate. Basically, copper atoms may produce chemical bonds with unfettered matrix atoms, specifically, with oxygen atoms. However, Cu–Cu bonding is energetically more favorable, as can be judged from the change in the Gibbs free energy in comparison with copper–oxygen reaction. Similar situation is observed with silver atoms in silver-doped silica glass [90].

In view of the fact that copper atoms readily combine with each other, an excess of the copper amount over the solubility limit of metal in Al_2O_3 leads to the formation of copper nanoparticles in the ion-implanted layer. As was noted earlier, the model approach based on binary atomic collisions in a homogeneous amorphous medium of oxide aluminum (which is involved in the DYNA algorithm) becomes inefficient when the dielectric substrate contains fragments of the metal phase [87]. However, the curves calculated at a low dose of $2.7 \cdot 10^{15}$ ion/cm^2 (Fig. 8) may be helpful in predicting the MNP distribution across the sample at higher doses. Consider the formation and distribution of MNPs at higher doses.

Note that an increase in the absolute copper ion concentration in the depth profiles and the surface sputtering coefficient depend on the implantation time (or the time of implant accumulation) [87]. Therefore, the particle nucleation and growth are time-dependent processes and will also vary with time with depth distribution. Generally, the ion synthesis of MNPs proceeds in several steps: (i) accumulation of Cu^0 atoms in a local near-surface area of sapphire, (ii) supersaturation of this area by Cu^0 atoms, (iii) formation of nuclei consisting of several Cu^0 atoms, and (iv) growth of the nanoparticles from the nuclei. Assuming that the MNP growth occurs by successive joining of the single Cu^0 atoms one can believe that this process is governed by both the local concentration of metal atoms and their diffusion mobility. Obviously, the size of nanoparticles forming at a certain depth from the surface correlates with the filling factor of the metal in the dielectric at the same depth, since they are both depend on the ion concentration profile. Therefore, bearing in mind the asymmetric copper atom distribution obtained for the maximal dose used in the calculations (Fig. 7), one can conclude that when this dose is exceeded and the distribution becomes asymmetric, the larger copper particles (and, accordingly, higher fill factors) will be observed near the Al_2O_3 surface, while finer nanoparticles will penetrate deeper into the matrix.

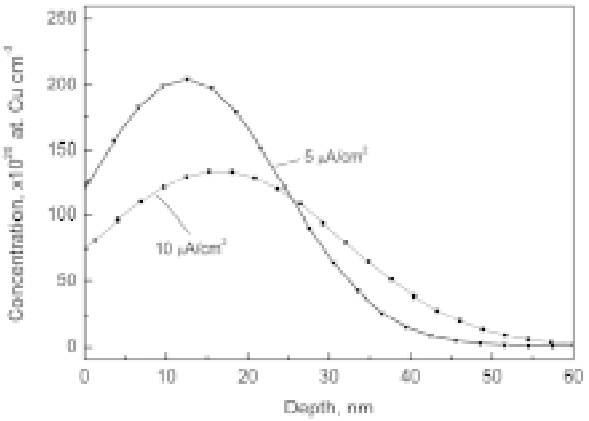

Fig. 9. Depth profile of the Cu^+-ion distribution for 40 keV implantation into Al_2O_3 at dose of $1.0 \cdot 10^{17}$ ion/cm^2 and two ion beam current densities, evaluated from RBS spectra.

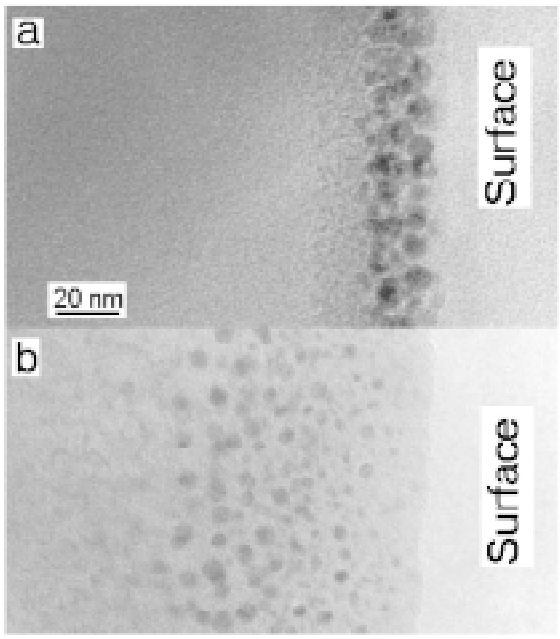

Fig. 10. Cross-sectional TEM micrographs obtained for Co+ ion implantation into silica with dose of 1.0 10^{17} ion/cm^2 at various energies (a) 30 keV and 160 keV.

In present work, the model predictions regarding the copper distribution inward to the Al_2O_3 matrix have been corroborated experimentally. As example, Fig. 9 shows the RBS copper atom profiles near the surface of the sapphire corresponding to II with a dose of $1.0 \cdot 10^{17}$ ion/cm^2 at two ion current densities of 5 and 12 μA/cm^2. Note that the RBS method gives the distribution of only copper atoms over the volume, ignoring the possible presence of the volume metal phase. As seen in figure, in the experimental distributions obtained at two ion current values, the copper concentration reaches a maximum near the surface (~ 10-20 nm in depth), decreasing monotonically with depth down to 60 nm. These asymmetrical profiles are in qualitative agreement with the curves shown in Fig. 7. The discrepancy in the positions of the maxima for two ion current values will be discussed below.

Similar distributions of MNPs in depth were also obtained in experiments on high-dose low-energy implantation of ions into other dielectrics; this follows from electron microscopy data for soda–lime silicate glass (SLSG) with MNPs [3,91], for copper particles in SiO_2 glass [92] or in Co-ion implanted silica [93] and also from the comparison measurements of the reflection from the implanted and back sides of silicate glasses substrates with silver particles [91,94,95].

As illustrated by cross-sectional transmission electron microscopy (TEM) analysis in Fig. 10 [93] and disused in [96], the distribution of MNPs synthesized by low-energy implantation is essentially different from distribution particles created by high-energy II. In former case, MNPs are distributed in the volume of the substrate with an almost symmetrical depth distribution.

Measured optical reflectance spectra of Cu-implanted Al_2O_3 for different ion current densities are represented in Fig. 11 [38]. The wide reflection bands in the visible range directly indicate the formation of copper nanoparticles in the sapphire volume. These bands are attributed to SPR localized in the small metal particles [65]. By comparing electron microscopic and optical data for MNPs synthesized by different techniques, it was shown that this optical resonance, which is due to collective oscillations of free electrons, is observed in the visible range when the size of copper particles lies between ~2 nm and several tens of nanometers [65]. Such reflection spectra are typical of copper particles in an dielectric matrix.

As seen in Fig. 11, for the lowest current density of 2.5 μA/cm^2, the reflectance peak is positioned at 610 nm with an intensity of 27%, implying the formation of small copper particles. Increasing the ion current density shifts the reflectance peaks to longer wavelengths (up to ~640 nm) and the intensity reaches 41% for 12.5 μA/cm^2. These spectral changes correspond to the formation of larger Cu particles. Similar optical effects were detected

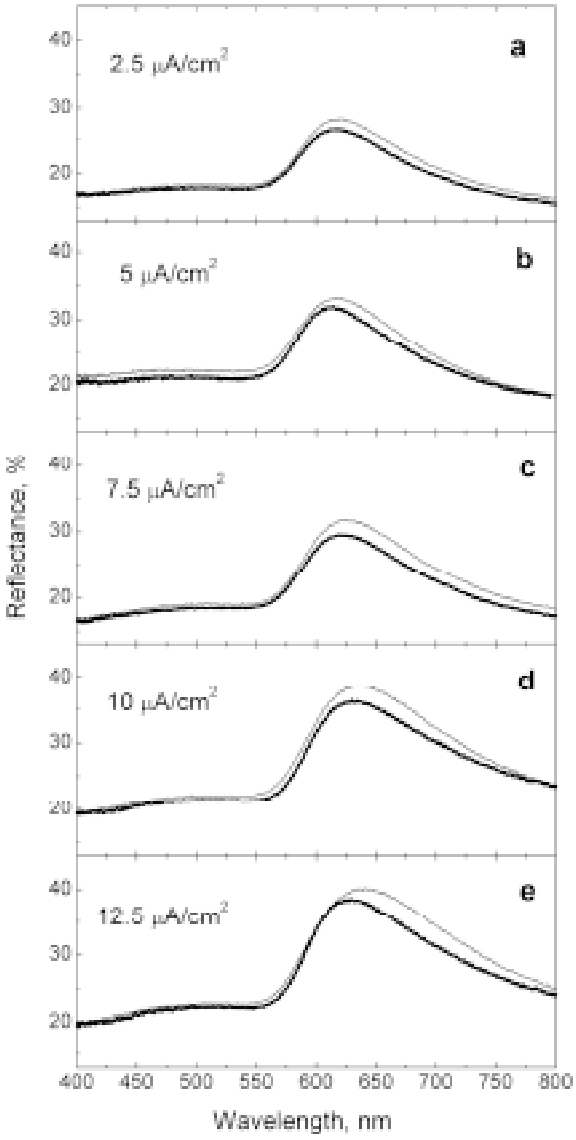

Fig. 11. Optical reflectance spectra of Al_2O_3 samples after Cu^+ ion implantation with fixed dose of $1.0 \cdot 10^{17}$ ion/cm^2 at various ion current densities (thin lines) and spectra taken from the same samples subjected to post-implantation laser annealing (thick lines) [38].

in the case of silver nanoparticles in SiO_2 fabricated at different current densities [97].

X-ray spectroscopy is a valuable tool for qualitative and quantitative element analysis. Each element has characteristic peak positions corresponding to the possible transitions in its electron shell. In present case, the presence of copper in sapphire is indicated by K-peak at about 8.0 keV (Fig. 12). The RBS and EDX data, suggest that the II leads to formation of copper particles at different current densities in approximately the same region of 50-60 nm in the depth for all implanted samples.

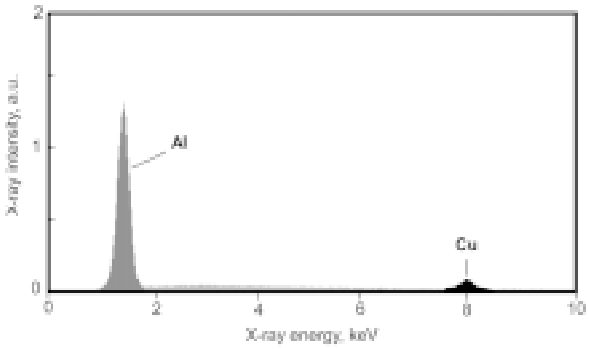

Fig. 12. Example of EDX spectrum of Al_2O_3 implanted with Cu^+ ions at an ion current density of 7.5 μA/cm^2.

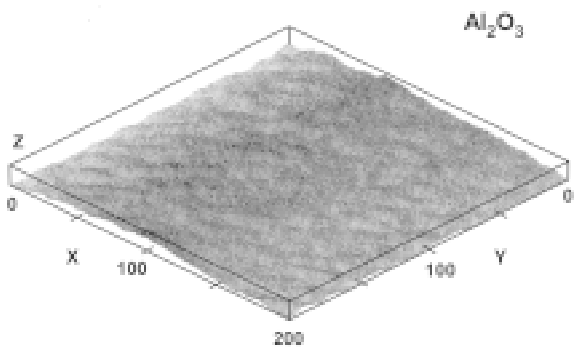

Fig. 13. AFM image of the surface of Al_2O_3 before ion implantation. The values plotted in the X and Y axes are given in nanometers. The step in the Z direction is 20 nm.

The AFM images of the non-implanted Al_2O_3 and same substrate after Cu^+ implantation at an ion beam current density of 7.5 μA/cm^2 are shown in Figs. 13 and 14 [40,41]. The formation of copper nanoparticles at the implanted surface is observed in AFM as semi-spherical hillocks of mean size 20 nm, which are absent on the nearly smooth surface of virgin Al_2O_3. These hillocks seen in Fig. 14 result from surface sputtering of Al_2O_3 during II and are merely the striped tops of spherical-shaped MNPs nucleated in the near-surface layer of the substrate. It is assumed that sapphire is removed (sputtered) with a higher rate than the metallic phase. Estimates [86,87] made for high-dose copper implantation into sapphire show that the Al_2O_3 layer sputtered may be several nanometers thick for the doses and energies considered in this work. For Cr^+ and Ti^+ implantation into sapphire (with a dose of ~ $1.0 \cdot 10^{17}$ ion/cm^2), the thickness of the layer sputtered from

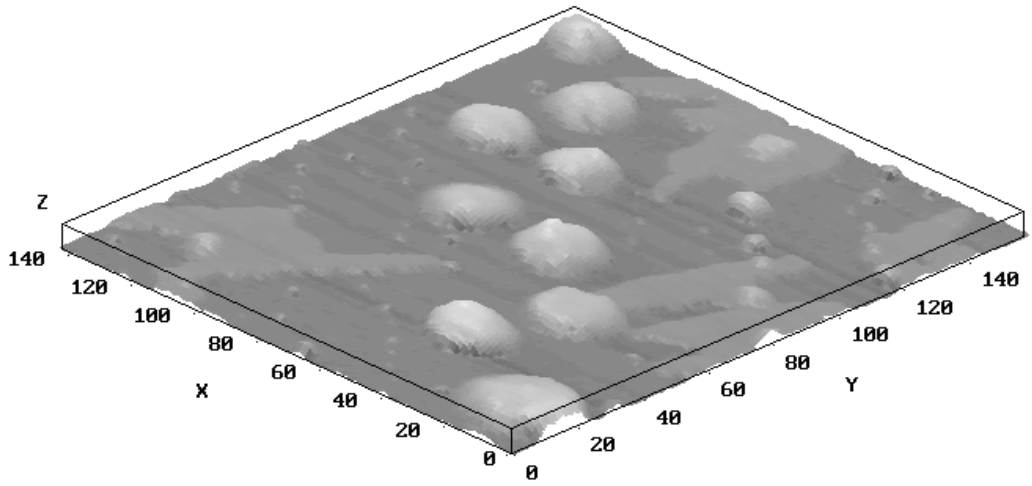

Fig. 14. AFM image of a fragment of the surface of Al_2O_3 implanted with Cu^+ ions at an ion current density of 7.5 μA/cm^2. The values plotted in the X and Y axes are given in nanometers. The step in the Z direction is 24 nm [40,41].

the sapphire surface was the value of same order (Fig. 5). Similar surface morphology with MNPs were earlier detected by AFM on the samples after low-energy (<60 keV) high-dose II, for example: Au^+ into Al_2O_3 [51] and mica [98]; Fe^+ into SiO_2 [99]; and Ag^+ into Al_2O_3, Ta_2O_3, Si_3N_4, SiO_2 [48,97,100], and in SLSG [4,101].The metal phase of nanoparticles on the surface was identified by glancing incidence X-ray diffraction (GIXRD) [100].

The attenuation (extinction) of an optical wave propagating in a medium with MNPs depends on the amount of the SPR effect and the light scattering efficiency. The wavelength of optical radiation, the particle size, and the properties of the environment are governing factors in this process. Within the framework of classical electrodynamics (the Maxwell equations), the problem of interaction between a plane electromagnetic wave and a single spherical particle was exactly solved in terms of optical constants of the interacting objects by Mie [102,103]. In the general case, the Mie electromagnetic theory imposes no limitations on the wavelength of optical radiation. Therefore, the operation on the optical constants of the particles and matrix results in extinction spectra, so-called Mie resonance bands [65], which agree well experiment. However, the Mie theory, which relies on the spectral dependence of the optical constants, does not allow one to penetrate deep into the physics of Mie optical peaks exhibited by the particles. Yet, independent investigations [65] into the behavior of metal nanoparticles showed that Mie resonances are due to the SPR effect, so that analytical Mie spectra may be compared with experimental data. Therefore, the Mie equations will be used to simulate the extinction spectra for copper nanoparticles in Al_2O_3 and the model spectra obtained will be compared with the experiment (Fig. 11), as was successfully done previously for silver particles synthesized in polymers by II [104]. In the calculations described below, we used the complex optical constants for Al_2O_3 [105] and copper [106] corrected for size effects (limitations imposed on the free path of electrons) observed in particles of size ranging from 1 to 200 nm (this range is somewhat wider than in Fig. 14).

Simulated extinction spectra for copper nanoparticles embedded in Al_2O_3 matrix for comparison them with experimental data shown in Fig. 15. These spectra feature a wide band, which covers the entire spectral range. In the given range of particle sizes, the position of the SPR absorption maximum shifts toward longer wavelengths with increasing particle size. Simultaneously, the intensity of the extinction band grows and the spectra somewhat broaden, which is in agreement with the changes in the experimental spectra with increasing ion current (Fig. 11). Such behavior of the reflection spectra confirms the statement that copper particles in sapphire grow with ion beam current density.

The most plausible reason for the increasing of the particles is that implantation rises the temperature of the Al_2O_3 matrix. For example, as was shown before [97], when low-energy Ag^+ ions were implanted into preheated (from 20 to 60° C) silica

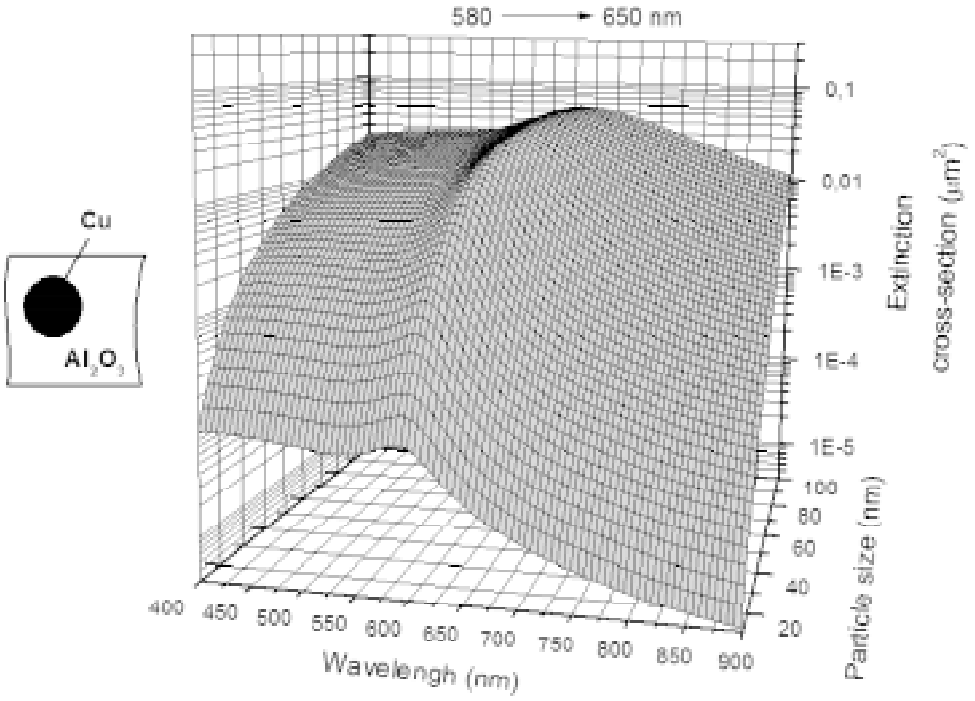

Fig. 15. Calculated spectra of optical extinction cross-section for copper nanoparticles embedded in Al_2O_3 vs. particle size.

glasses at a moderate ion current density of 3 mA/cm^2, larger silver particles were formed in warmer samples. It is obvious that an increase in the substrate temperature accelerates diffusion mobility of the implants and increases a probability for nucleation and growth of MNPs.

As was noted earlier, the process of MNP synthesis may be subdivided into steps including the incorporation of the accelerated ions, their diffusion, the nucleation and growth of particles. In our case, however, all the samples were kept under identical conditions (i.e., at room temperature) prior to beginning of II. It appears that different values of the ion current density result in different rates of incorporation of copper ions into the matrix, which deliveries the energy from the implant and heats up Al_2O_3. Thus, we may conclude that the higher is the ion current density the higher are the heating rate (temperature gradient) and the temperature of the substrate. So one can consider the process as temperature-enhanced diffusion of implants in substrates at high-beam-current II. At elevated temperatures and temperature gradients in the Al_2O_3 matrix, the diffusion mobility of copper ions in substrate grows, the ions drain faster toward nuclei that have already formed, and as result the size of the MNPs increases (diffusion growth). In 'hot' samples, the amount of ions unattached to the particles, i.e., remaining dispersed in the implanted layer, is smaller than in 'cold' ones. Ostwald ripening could also contributes to the increasing of the particles: fine nuclei, which have a lower melting point, dissociate into atoms, which serve as building blocks for other (large) particles. As a result, the total number of the MNPs decreases.

Under the implantation conditions used in our experiments, the matrix temperature was not so high that the extremely intense diffusion flux of embedded copper atoms inward to the matrix could prevent particle nucleation. However, as follows from the RBS spectra in Fig. 9, the high ion current rises the copper ion mobility and the RBS spectrum becomes smeared. In addition, its maximum slightly shifts inward to the substrate, which is one more indication that the copper ion mobility in this matrix is enhanced.

Broadening of the RBS spectrum implies a wide distribution in the particle size across the depth. Therefore, it would be of interest to estimate the feasibility of modifying implantation-synthesized MNPs by means of laser annealing. This issue is considered in the next section.

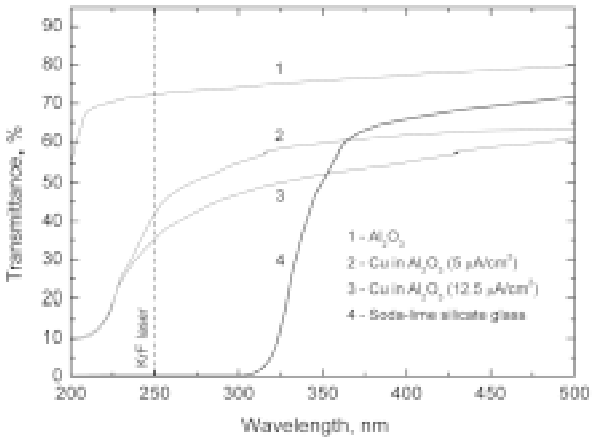

Fig. 16. Optical transmission spectra of Al_2O_3 before and after copper implantation for different values of the ion beam current density. The spectrum for non-irradiated SLSG is given for comparison.

5. MODIFICATION OF METAL NANOPARTICLES IN SAPPHIRE BY LASER ANNEALING

In the earlier study on annealing of ion-implanted structures by an excimer laser (see review [73]), the main feature of the experiments was that the laser pulses were applied in UV spectral area, which falls into the range of strong absorption by dielectrics (for example, in the case of SLSG containing implanted silver nanoparticles). Such annealing usually leads to melting of the glass near surface layer, including the implanted MNPs, followed by rapid cooling. As a result, the size of the silver nanoparticles diminishes, because the heat of the matrix, which intensely heats up, melts the particles. Melting is favored by a relatively low melting point of the SLSG (~750 °C), application of high-power laser pulses, and also the fact that the melting point of small silver particles is close to the melting point of the glass [73,107].

In present work, the similar approach was applied to modify copper nanoparticles implanted in Al_2O_3 using an excimer laser. However, the melting point of artificial sapphire is higher (1400 °C) than that of SLSG and sapphire is more transparent at the KrF laser radiation wavelength of 248 nm (Fig. 16). Therefore, one can assume that the laser radiation absorption in sapphire is lower than in the glass and consider the annealing process as direct interaction between laser light and MNPs irrespective of the substrate temperature.

As seen in Fig. 16, the optical transmission of Al_2O_3 in the UV spectral range decreases after II because of induced radiation defects of matrix [3]. Yet, the matrix remains quite transparent (35–40%) near the laser wavelength especially versus the transmission of SLSG of the same thickness. It should be noted that synthesized copper nanoparticles also slightly absorb UV light due to interband transitions just as in the bulk metal [65].

The reflection optical spectra of the implanted samples subjected to laser annealing are shown by thick lines in Fig. 11. These selective bands indicate that the MNPs are present in the sapphire after the annealing as well. However, in all the samples, the maxima of these reflection SPP bands turn out to be shifted toward shorter wavelength and they are less intense than in the spectra taken immediately after implantation. These changes are more pronounced in the case of high-current II; in other words, for samples with large copper particles are more sensitive to laser radiation that fine particles, which were synthesized at low current densities. Reduction of the intensity of the spectral bands for annealed samples in present study is smaller than it was earlier registered for copper and silver nanoparticles formed by II in SLSG and treated by laser under similar conditions [66,73,108].

In terms of the Mie theory, which describes the optical properties of small metal particles (see the previous section, Fig. 15), the shift of the reflection maxima to shorter wavelength means that laser annealing of sapphire decreases the mean size of the copper particles. This conclusion is corroborated by AFM examinations. In fact, the hillocks seen in the surface image after II Fig. 14) are large than those observed after II and laser annealing (Fig. 17) at least by one order of magnitude.

The mechanisms of interaction of high power laser radiation with composite materials depend on the parameters of the laser beam and the physicochemical properties of the annealed material. In general, the laser processes are determined by photoexcitation relaxation time. In the case of metal-dielectric composite, corresponding processes of excitation and relaxation can be separated between effects in sapphire matrix and in the MNPs. Despite of the fact that sapphire matrix has an energy bandgap at ~ 9.9 eV, irradiation with a high power excimer laser at the wavelength of 248 nm (5 eV) couples directly through the spectral absorption edge of Al_2O_3 (Fig. 16), Therefore, the radiation generates electron–hole pairs in Al_2O_3 by direct exiting electrons from the valence into the conduction band.

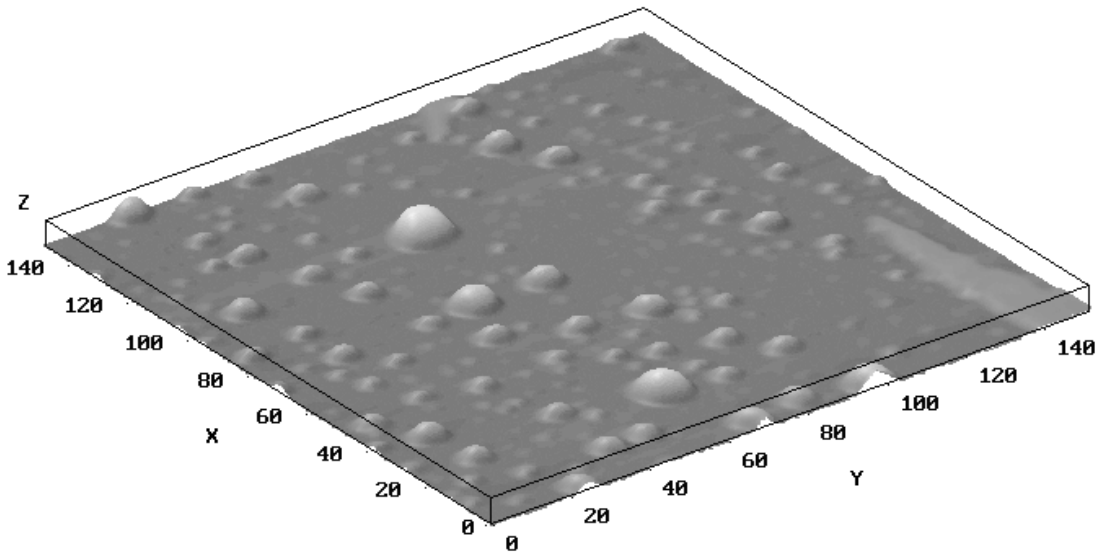

Fig. 17. AFM image of a fragment of the surface of Al_2O_3 implanted with Cu^+ ions at an ion current density of 7.5 μA/cm^2 after laser annealing. The values plotted in the X and Y axes are given in nanometers. The step in the Z direction is 48 nm [40,41].

In the copper particles, both conduction- and valence-band electrons may participate in the laser excitations at the same wavelength. In other words, the number and energy of absorbed photons immediately establishes the temperature rise in a laser-irradiated metal, whereas the number of valence-to-conduction-band excitations establishes the initial density of electron-hole pairs in an dielectric [109]. In a metal, the time between electron–electron collisions is of the order of 10^{-14} – 10^{-13} s and electron–phonon relaxation are typically one or two orders of magnitude slower [110]. In non-metal, interband electronic excitations range from 10^{-12} to 10^{-6} s [109].

Overall, most of this times are short in comparison with the pulse duration (25 ns) of the laser described here; so the laser energy can be assumed as converted directly into a heating of the MNPs. Therefore, although Al_2O_3 is considered as almost transparent to the laser light (Fig. 16), a fraction of the radiation is still absorbed by the sapphire matrix. However, it may be roughly assumed that most of the energy of the laser radiation is absorbed by the MNPs and the transparent substrate has no time to heat up. Thus, the decrease in the metal nanoparticle size observed in the experiment (Figs. 13,14,17) may be due to photofragmentation suggested for laser irradiated small silver particles [111]. This process means a decrease in the total number of the particles in the substrate when some of them disintegrate into atoms or tiny molecule-like clusters, which do not exhibit SPR-related absorption. Clearly, large MNPs, which have a larger volume and cross-sectional area and, therefore, absorb a greater amount of the laser energy, are more prone to fragmentation. Especially, the larger particles are responsible for the reduction of the SPR band intensity and their shift to shorter wavelength when they disintegrated. Earlier, metal particle fragmentation was observed in colloidal solutions exposed to high-power picosecond or nanosecond laser shorts at wavelengths outside the SPR spectral range of MNPs [111–113]. It was assumed that fragmentation takes place when the laser radiation causes electrons to move to the periphery of the particles, which thereby acquire an appreciable surface charge (Fig. 18) [111].

On the other hand, the conversion of the laser radiation in metal particles may be treated as the photon energy transformation (relaxation) directly into heating of the MNPs in composite. The temperature may rise to the melting point of copper particles, since it is known that the melting point of a metal particle may drop substantially when its size decreases to the nanometer scale from the bulk [114,115]. For example, it was reported that the melting point of silver particles less than 50 nm

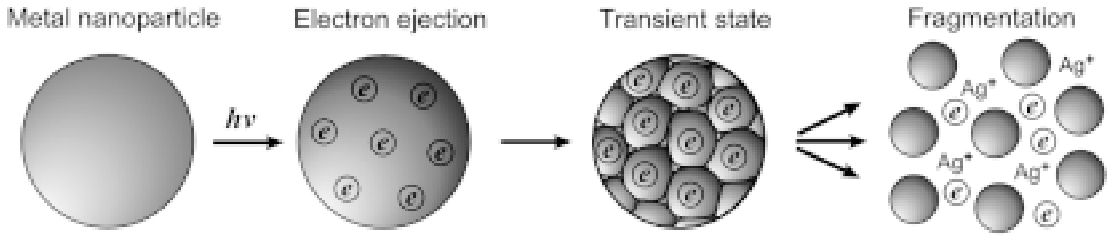

Fig. 18. Stages of metal particle fragmentation with laser excitation. A transient aggregate formed via the photoejection of electrons is considered to be a precursor for complete fragmentation of the particle. This picture with improved contrast was taken from [111].

in size declined to ~500 °C (cf. the melting point of bulk silver, 960 °C) [116,117]. Consequently, when the temperature of the particles exceeds their melting point, they melt, diminish, and may even collapse. In general, melting of nanoparticles is a nontrivial process and its correct description requires that several sequential stages be considered: surface atom migration (surface premelting), structure fluctuations (quasi-melting), and the formation of mixed (liquid–solid) phases. This effect is dependent on the particle size, and so smaller particles will decrease faster than lager ones. In general, a common decrease in the particle sizes of all particles by a given melting mechanism will be reflected in the optical spectra in the same way as in photofragmentation. Therefore, it is as yet difficult to decide between the two mechanisms of particle decrease at laser annealing. The difference between them is that fragmentation breaks down primarily larger particles, while fine particles are more prone to melting. Fragmentation seems to be a more vigorous process and possibly is responsible for the changes observed at laser annealing.

ACKNOWLEDGEMENTS

A.L.S. is grateful to the Alexander Humboldt Foundation for the financial support of his work in Germany and Austrian Scientific Foundation in the frame of Lise Meitner Program. This study was sponsored in part by the Federal Program for Support of the Leading Scientific Schools of Russia (grant no. NSh 1904.2003.2), the Russian Foundation for basic Research (grant no. 04-02-97505) and the OFN RAN program 'Advanced Materials and Structures'. Special thanks to V.F. Valeev, V.I. Nuzhdin, R.I. Khaibullin, Yu.N. Osin and S.N. Abdullin for the assistance in carrying out implantation and electron microscopy study and also to V. Hnatowicz and V.N. Popok for taking RBS spectra.

REFERENCES

[1] C. Flytzanis, F. Hache, M. C. Klein, D. Ricard and P. Rousignol, *Nonlinear optics in composite materials* (Elsevier Science, Amsterdam, 1991).
[2] A.L. Stepanov, I.B. Khaibullin, P.D. Townsend, D.E. Hole and A.A. Bukharaev, *Rus. Feder. Patent* No. 2156490, 2000.
[3] P.T. Townsend, P.J. Chandler and L. Zhang, *Optical effects of ion implantation* (Cambridge Univ. Press, Cambridge, 1994).
[4] A.L. Stepanov and D.E. Hole,In: *Recent Research Development Applied Physcs Vol. 5,* ed. by S.G. Pandalai (Transworld Research Network, Kuala, 2002) p. 1.
[5] A. Polman // *J. Appl. Phys.* **82** (1997) 1.
[6] J. Davenas, A. Perez, P. Thevenard and C.H.S. Dupuy *// Phys. Stat. Sol. A* **19** (1973) 679.
[7] M. Treilleux, P. Thevenard, G. Ghassagne and L.H. Hobbs *// Phys. Stat. Sol. A* **48** (1978) 425.
[8] C.J. McHargue, G.C. Farlow, P.S. Sklad, C.W. White, A. Perez, N. Kornilios and G. Marest // *Nucl. Instr. Meth. B* **19-20** (1987) 813.
[9] C.J. McHargue, P.S. Sklad and C.W. White // *Nucl. Instr. Meth. B* **46** (1990) 79.
[10] C.J. McHargue, P.S. Sklad, C.W. White, G.C. Farlow, A. Perez and G. Marest // *J. Mater. Res.* **6** (1991) 2145.
[11] C.J. McHargue, S.X. Ren, P.S. Sklad, L.F. Allard and J. Hunn // *Nucl. Instr. Meth. B* **166** (1996) 173.

[12] C.J. McHargue, S.X. Ren and J.D. Hunn // *Mat. Sci. Eng. A* **253** (1998) 1.
[13] M. Ohkubo, T. Hioki and J. Kawamoto // *J. Appl. Phys.* **62** (1987) 3069.
[14] M. Ohkubo, T. Hioki, N. Suzuki, T. Ishiguro and J. Kawamoto // *Nucl. Instr. Meth. B* **39** (1989) 675.
[15] G.C .Farlow, P.S. Sklad, C.W. White and C.J. McHargue // *J. Mater. Res.* **5** (1990) 1502.
[16] C. Donnet, G. Marest, N. Moncoffre, J. Tousset, A. Rahioui and C. Esnouf // *Nucl. Instr. Meth. B* **59-60** (1991) 1205.
[17] P.S. Sklad, C.J. McHargue, C.W. White and G.C. Farlow // *J. Mat. Sci.* **27 (**1992) 5895.
[18] H.-G. Jang, H.-B. Kim, J.-H. Joo, C.-N. Whang, H.-K. Kim, D.-W. Moon, J.J. Woo and S.-O. Kim // *Nucl. Instr. Meth. B* **124** (1997) 528.
[19] T. Kobayashi and T. Terai // *Nucl. Instr. Meth. B* **141** (1998) 441.
[20] T. Kobayashi, A. Nakanishi, K .Fukumura and G. Langouche // *J. Appl. Phys.* **83** (1998) 4631.
[21] I. Sakamoto, S. Honda, H. Tanoue, N. Hayashi and H. Yamane // *Nucl. Instr. Meth. B* **148** (1999) 1039.
[22] N. Hayashi, T. Toriyama, H. Wakabayashi, I. Sakamoto, T. Okada and K. Kuriyama // *Nucl. Instr. Meth. B* **158-159** (2002) 193.
[23] H. Wakabayashi, T. Hirai, T. Toriyama, N. Hayashi and I. Sakamoto // *Phys. Stat. Sol.* **189** (2002) 515.
[24] E. Alves, C. MacHargue, R.C. da Silva, C. Jesus, O. Conde, M.F. da Silva and J.C. Soares // *Surf. Coat.. Tech.* **128-129** (2002) 434.
[25] T. Monteiro, C. Boemare, M.J. Soares, E. Alves, C. Marques, C. McHargue, L.C. Ononye and L.F. Allard // *Nucl. Instr. Meth. B* **191** (2002) 638.
[26] C.W. White, S.P. Withrow, K.D. Sorge, A. Meldrum, J.D. Budai, J.R. Thompson and L.A. Boatner // *J. Appl. Phys.* **93** (2003) 5656.
[27] C.J. McHargue, L.C. Ononye, E. Alves, C. Marques and L.F. Allard // *Nucl. Instr. Meth. B* **218** (2004) 227.
[28] Y. Saito, H. Horie and S. Suganomata // *Nucl. Instr. Meth. B* **59-60** (1991) 1173.
[29] C. Marques, M.M. Cruz, R.C. da Silva and E. Alves // *Nucl. Instr. Meth. B* **175-177** (2001) 500.
[30] C. Marques, M.M. Cruz, R.C. da Silva and E. Alves // *Surf. Coat. Tech.* **158-159** (2002) 54.
[31] A. Meldrum, L.A. Boatner and K. Sorge // *Nucl. Instr. Meth. B* **207** (2003) 36.
[32] T. Kobayashi, T. Terai, T. Yoneoka and S. Tanaka // *Nucl. Instr. Meth. B* **116** (1996) 187.
[33] X. Xiang, X.T. Zu, S. Zhu and L.M. Wang // *Appl. Phys. Lett.* **84** (2004) 52.
[34] X. Xiang, X.T. Zu, S. Zhu and L.M. Wang // *Mat. Res. Soc. Symp. Proc.* **792** (2004) R9.9.1.
[35] D. Ila, E.K. Williams, S. Sarkisov, D.B. Pocker, D.K. Hensley, C. Klatt and S. Kalbitzer // *Mat. Res. Soc. Symp. Proc.* **504** (1998) 381.
[36] M. Ikeyama, S. Nakao, M. Tazawa, K. Kadono and K. Kamada // *Nucl. Instr. Meth. B* **175-177** (2001) 652.
[37] M. Ikeyama, S .Nakao and M. Tazawa // *Surf. Coat. Tech.* **158-159** (2002) 720.
[38] A.L. Stepanov, U. Kreibig, D.E. Hole, R.I. Khaibullin, I.B. Khaibullin and V.N. Popok // *Nucl. Instr. Meth. B* **178** (2001) 120.
[39] A.L. Stepanov // *Tech. Phys. Lett.* **28** (2002) 864.
[40] A.L. Stepanov, V.N. Popok, D.E. Hole and I.B. Khaibullin // *Appl. Phys. A* **74** (2002) 441.
[41] A.L. Stepanov and V.N. Popok // *AIP Conf. Proc.* **680** (2003) 601.
[42] A.L. Stepanov // *Tech. Phys.* (2005) *in press*.
[43] G. Battaglin, R. Bertoncello, M. Casarin, E. Cattaruzza, G. Mattei, P. Mazzoldi, F. Trivillin and M. Urbani // *J. Non.-Cryst. Solids* **253** (1999) 251.
[44] M. Rahmani; L.H. Abu-Hassan, P.D. Townsend, I.H. Wilson and G.L. Destefanis // *Nucl. Instr. Meth. B* **32 (**1988) 56.
[45] M. Rahmani and P.D. Townsend // *Vacuum* **39** (1989) 1157.
[46] C.W. White, D.K. Thomas, R.A Zuhr, J.C. McXallum, A. Pogany, R.H. haglund, R.H. Magruder III and L. Yang // *Mater. Res. Soc. Proc*. **258** (1992) 331.
[47] C.W. White, D.K. Thomas, D.K. Hensley, R.A. Zuhr, J.C. McCallum, A. Pogany, R.F. Haglund, R.H. Magruder and L. Yang // *Nanostrust. Mat.* **3** (1993) 447.
[48] G. Steiner, M.T. Pham, C. Kuhne and R. Salzer // *Fresenius J. Anal. Chem.* **362** (1998) 9.

[49] E. Alves, R.C. da Silva, O. Conde, M.F. da Silva and J.C. Soares // *Nucl. Instr. Meth. B* **148** (1999) 1049.
[50] M. Ohkubo and N. Suzuki // *Phil. Mag. Lett.* **57** (1988) 261.
[51] D.O. Henderson, R. Mu, M.A. George, A. Burger, S.H. Morgan, C.W. White, R.A. Zuhr and R.H. Magruder III // *J. Vac. Sci. Technol. B* **13** (1995) 1198.
[52] C. Marques, E. Alves, R.C. da Silva, M.R. Silva and A.L. Stepanov // *Nucl. Instr. Meth. B* **218** (2004) 139.
[53] S. Dhara, B. Sundaravel, T.R. Ravindrn, K.G.M. Nair, C. David, B.K. Panigrahi, P. Magudapathy and K.H. Chen // *Chem. Phys. Lett*. **399** (2004) 354.
[54] N. Can, P.D. Townsend and D.E. Hole // *Appl. Phys. Lett.* **65** (1994) 1871.
[55] N. Can, P.D. Townsend, D.E. Hole, H.V. Snelling, J.M. Ballesteros and C.N. Afonso // *J. Appl. Phys.* **78** (1995) 6737.
[56] N. Hayashi, I. Sakamoto, H. Wakabayashi, T. Toriyama and S. Honda // *J. Appl. Phys*. **94** (2003) 2597.
[57] C.E. Vallet, C.W. White, S.P. Withrow, J.D. Budai, L.A. Boatner, K.D. Sorge, J.R. Thompson, K.S. Beaty and A. Meldrum // *J. Appl. Phys*. **92** (2002) 6200.
[58] C.W. White, S.P. Withrow, J.D. Budai, L.A. Boatner, K.D. Sorge, J.R. Thompson, K.S. Beaty and A. Meldrum // *Nucl. Instr. Meth. B* **191** (2002) 437.
[59] S.P. Withrow, C.W. White, J.D. Budai, L.A. Boatner, K.D. Sorge, J.R. Thompson and R. Kalyanaraman // *J. Mag. Mag. Mat.* **260** (2003) 319.
[60] G.C. Farlow, P.S. Sklad, C.W. White and C.J. McHargue // *J. Mater. Res*. **5** (1990) 1502.
[61] T. Miyano, T. Matsumae, Y. Yoko-o, M. Kiuchi and M. Satou // *Nucl. Instr. Meth. B* **59-60** (1991) 1167.
[62] T. Futagami, Y. Aoki, O. Yoda and S. Nagai // *Nucl. Instr. Meth. B* **88** (1994) 261.
[63] J. Bigarre, S. Fayeulle, D. Treheux and N. Moncoffre // *J. Appl. Phys.* **82** (1997) 3740.
[64] T. Kobayashi and T. Terai // *Nucl. Instr. Meth. B* **148** (1999) 1059.
[65] U. Kreibig and M. Vollmer, *Optical properties of metal clusters* (Springer-Verlag, Berlin, 1995).
[66] R.W. Wood, P.D. Townsend, N.D. Skelland, D.E. Hole, J. Barton and C.N. Afonso // *J. Appl. Phys*. **74** (1993) 5754.
[67] A.L. Stepanov, D.E. Hole, A.A. Bukharaev, P.D. Townsend and N.I. Nurgazizov // Appl. Surf. Sci. **136** (1998) 298.
[68] A.L. Stepanov, D.E. Hole and P.D. Townsend // *Nucl. Instr. Meth. B* **149** (1999) 89.
[69] A.L. Stepanov and V.N. Popok // *J. Appl. Spectr.* **68** (2001) 164.
[70] A.L. Stepanov, V.N. Popok, D.E. Hole and A.A. Bukharaev // *Phys. Soid. State* **43** (2001) 2192.
[71] A.L. Stepanov // *Phil. Mag. Lett.* **82** (2002) 149.
[72] A.L. Stepanov // *Rev. Adv. Mater. Sci.* **4** (2003) 123.
[73] A.L. Stepanov, In: *Recent Research Development in Non-Crystlline Solids Vol. 3,* ed. by S.G. Pandalai (Transworld Research Network, Kuala, 2003) p. 177.
[74] N.P. Barradas, C. Jeynes and R.P. Webb // *Appl. Phys. Lett.* **71** (1997) 291.
[75] J.D. Demaree, S.R. Kirkpatrick, A.R. Kirkpatrick and J.K. Hirvonen // *Nucl. Inst. Meth. B* **127-128** (1997) 603.
[76] C.G. Lee, Y. Takeda, N. Kishimoto and N. Umeda // *J. Appl. Phys.* **90** (2001) 2195.
[77] V.B. Odzhaev, I.P. Kozlov, V.N. Popok and D.V. Sviridov, *Ion implantation into polymers* (Belarusk. Gos. Univ., Minsk, 1998), in Russian.
[78] G.G. Zakirov, Khaibullin I.B. and M.M. Zaripov // *Sov. Phys. Semmicond.-USSR* **17** (1983) 150.
[79] R.H. Magruder III, R.F. Haglund Jr., L. Yang, J.E. Wittig and R.A. Zuhr // *J. Appl. Phys.* **76** (1994) 708.
[80] S. Deying, Y. Saito and S. Suganomata // *Jpn. J. Appl. Phys.* **33** (1994) L966.
[81] A.L. Stepanov, S.N. Abdullin, R.I. Khaibullin, V.F. Valeev, Yu.N. Osin, V.V. Bazarov and I.B. Khaibullin // *Mater. Res. Soc. Symp. Proc.* **392** (1995) 267.
[82] V.N. Popok, R.I. Khaibullin, A. Toth, V. Beshliu, V.Hnatowicz and A. Mockova // *Surf. Sci.* **532-535** (2003) 1034.
[83] A.L. Stepanov, R.I. Khaibullin, S.N. Abdullin, Yu.N. Osin and I.B. Khaibullin // *Pros. Inst. Phys. Conf. Ser.* **147** (1995) 357.
[84] J. Bigarre, S. Fayeulle, D. Treheux and N. Moncoffre // *J. Appl. Phys.* **82** (1997) 3740.

[85] J.F. Ziegel, J.P. Biersak and U. Littmark, *The stopping and range of ions in solids* (Pergamon, N.Y., 1996).
[86] A.L. Stepanov, V.A. Zhikharev and I.B. Khaibullin // *Phys. Solid State* **43** (2001) 776.
[87] A.L. Stepanov, V.A. Zhikharev, D.E. Hole, P.D. Townsend and I.B. Khaibullin// *Nucl. Inst. Meth. B* **166-167** (2000) 26.
[88] V.M. Konoplev // *Rad. Eff. Lett.* **87** (1986) 207.
[89] V.M Konoplev // Poverkhost **2** (1986) 207, in Russian.
[90] P.W. Wang // *Appl. Surf. Sci.* **120** (1997) 291.
[91]L.C. Nistor, J. van Landuyt, J.D. Barton, D.E. Hole, N.D. Skelland and P.D. Townsend // *J. Non.-Cryst. Solids* **162** (1992) 217.
[92] N. Kishimoto, N. Umeda, Y. Takeda, C.G. Lee and V.T. Gritsyna // *Nucl. Instr. Meth. B* **148** (1999) 1017.
[93] O. Cíntora-González, D. Muller, C. Estournés, M. Richard-Plouet, R. Poinsot, J.J. Grob and J. Guille // *Nucl. Instr. Meth. B* **178** (2001) 144-147.
[94] A.L. Stepanov, D.E. Hole and P.D. Townsend // J. Non.-Cryst. Solids **244** (1999) 275.
[95] A.L. Stepanov // *Optics and spectrosopy* **89** (2000) 408.
[96] A.L. Stepanov, In: *Metal-Polymer nanocomposites* ed. by L. Nicolais and G. Garotenuto (John Wiley & Sons, Hoboken, 2005) p. 241.
[97] A.L. Stepanov and V.N. Popok // *Surf. Sci.* **566-568** (2004) 1250.
[98] D.O. Henderson, R. Mu., A. Ueda, Y.S. Tung, C.W. White, R.A Zuhr and J.G. Zhu // *J. Non.-Cryst. Solyds* **205-207** (1996) 788.
[99] A.A. Bukharaev, V.M. Janduganov, E.A. Samarsky and N.V. Berdunov // *Appl. Surf. Sci.* **103** (1996) 49.
[100] M.T. Pham, W. Matz and H. Seifarth // *Anal. Chim. Acta.* **350** (1997) 209.
[101] A.L. Stepanov, D.E. Hole, A.A. Bukharaev, P.D. Townsend and N.I. Nurgazizov *// Appl. Surf. Sci*. **136** (1998) 298.
[102] G. Mie // *Ann. Phys.* **25** (1908) 377.
[103] M. Born and E. Wolf, *Principles of optics* (Cambridge Univ. Press: Cambridge 1999).
[104] A.L. Stepanov, In: *Recent Research Development in Colloids and Interface Vol. 2,* ed. by S.G. Pandalai (Transworld Research Network, Kuala, 2004) p. 1.
[105] E.D.Palik*, Handbook of Optical Constants of Solids* (Academic Press, London, 1997).
[106] P.B. Johnson and R.W. Christy // *Phys. Rev. B* **6** (1972) 4370.
[107] A.L. Stepanov, D.E.Hole and P.D. Townsend // *J. Non.-Cryst. Solids* **260** (1999) 65.
[108] A.L. Stepanov, D.E.Hole and P.D. Townsend // *Nucl. Instr. Meth. Bs* **166-167** (2000) 882.
[109] D. Bauerle*, Laser processing and chemistry* (Springer, Berlin, 1996).
[110] J.Y. Bigot, J.C. Merle, O. Cregut and A. Daunois // *Phys. Rev. Lett.* **75** (1995) 4702.
[111] P.V. Kamat, M. Flumian and G.V. Harland // *J. Phys. Chem. B* **102** (1998) 3123.
[112] S. Link., C. Burda, M.B. Mohamed, B. Nikoobakht and M.A. El-Sayed // *J. Chem. Phys. B* **103** (1999) 1165.
[113] S. Link and M. A. El-Sayed // *Annu. Rev. Phys. Chem.* **54** (2003) 331.
[114] D. Dalacu and L. Martinu // *Appl. Phys. Lett.* **77** (2000) 4283.
[115] K. Dick, T. Dhanasekaran, Z. Zhang and D. Meisel // *J. Am. Chem. Soc.* **124** (2002) 2312.
[116] T. Castro, R. Reifenberg, E.Cho and, R.P. Andres // *Phys. Rev. B* **42** (1990) 8548.
[117] J. Roiz, A. Oliver, E. Munoz, L. Rodriguez-Fernandez, J.M. Hernandez and J.C. Chang-Wong // *J. Appl. Phys*. **95** (2004) 1783.